Multiwavelength study of the North Ecliptic Pole Field and Identification of candidate high-redshift galaxies

F. Mazyed,[1,2] D. Burgarella,[1] F.-T. Yuan,[3,1] N. Oi,[4] T. Goto,[5] and the *AKARI*-NEP team[6]

[1]*Aix Marseille Université, CNRS, LAM (Laboratoire d'Astrophysique de Marseille), UMR 7326, 13388, Marseille, France*
[2]*University of Wasit, 52001, Wasit, Iraq*
[3]*Shanghai Astronomical Observatory, China*
[4]*Tokyo University of Science, 1-3, Kagurazaka, Shinjuku-ku, Tokyo, 162-8601, Japan*
[5]*Institute of Astronomy, National Tsing Hua University, No. 101, Section 2, Kuang-Fu Road, Hsinchu, Taiwan 30013, R.O.C.*
[6]*coordinated by H. Matsuhara, ISAS, JAXA, Sagamihara, Kanagawa 229-8510, Japan*

ABSTRACT

Multi-wavelength data from the far-UV to the far-IR have been collected in the North Ecliptic Pole (NEP). These data are crucial to understand the galaxy populations detected in this study. More specifically, this work made use of *GALEX* data in far- and near-UV, SUBARU HSC data in the optical, *AKARI* and *WISE* data in the near- and mid-IR and *Herschel* data in the far-IR to try and identify a sample of candidate high-redshift, possibly lensed galaxies. From the list of candidates, we have obtained follow-up observations at IRAM/30m, NOEMA, Gemini North and SMA to better understand our galaxies. This work is the beginning of a promising project dedicated to the study of high-redshift galaxies in the NEP.

1. INTRODUCTION

Although studying individual galaxies can be quite informative, understanding a global phenomenon like the galaxy formation and evolution means that we need large galaxy samples. This theme needs statistics. This is one of the reasons why we build wide field surveys to collect large samples. Another one is because wide fields are necessary to detect and identify rare objects. The color-color selection method (aka dropout) has been used to build large samples of star-forming galaxies at $0.7 < z < 10$ (see e.g., Burgarella et al. 2007; Bouwens et al. 2016). Far-IR and sub-mm telescopes measured their dust properties up to $z \sim 4$ (Gruppioni et al. 2013; Burgarella et al. 2013). In this work, we have generated multi-band point source catalogs from observations of the NEP field with *GALEX*, and *Herschel*. Finally, to model and interpret this multi-wavelength dataset, we need an efficient and versatile tool able to physically model all the various components of a galaxy and the underlying physics. Here, we use CIGALE (Burgarella et al. 2005; Noll et al. 2009) which is available to the community (http://cigale.lam.fr) and supported by the authors.

2. MULTI-WAVELENGTH DATA: THE NEED FOR THE FAR-UV AND THE FAR-IR

Galaxies are complex systems that contain gas, dust, stars and sometimes an active galactic nuclei in their core. Physically modeling the emission of a galaxy implies that we are able to model all the physical processes occurring in a galaxy. These processes emit (or can emit) in different wavelength ranges covering the entire spectral energy distribution (SED) of galaxies. In this work, we perform an analysis from the far-UV to the far-IR, including *AKARI* and deep new SUBARU data (Figure 1) to identify and study high-redshift candidates that would show a red color in the far-IR. The negative K-correction leads to high-redshift galaxies being easier to detect at sub-millimeter wavelengths as compared with their low-redshift counterparts. We make use of the red colors as a selection and develop color criteria.

3. THE GRAVITATIONAL LENSING EFFECT

Gravitational lensing is the bending of light caused by a massive mass located between the source and the observer. In addition to providing an information on the lensed galaxy, gravitational lensing probes the total mass of the foreground lens, including the relative content of dark and luminous mass. One of the by-products of this work is to select out possible high-redshift candidates via their red far-IR colors. The magnification helps alleviating the photon starvation, and, facilitates follow-up observations of galaxies obscured by dust and in particular the determination of their redshift.

4. HIGH-REDSHIFT SUB-MILLIMETER GALAXIES

Corresponding author: Denis Burgarella
denis.burgarella@lam.fr

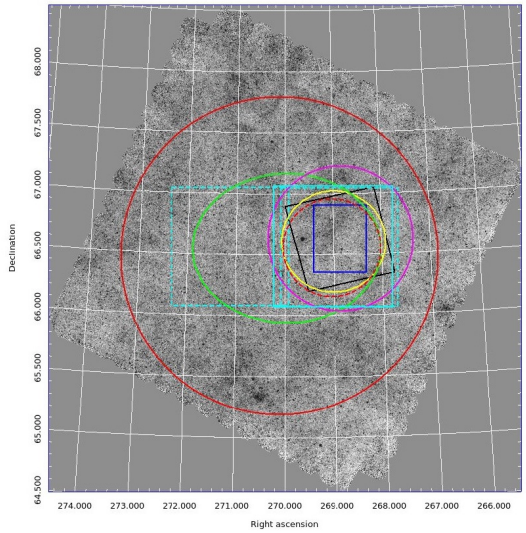

Figure 1. The area coverage of the NEP field. The background image is the *Herschel*/SPIRE 250 μm, the same area is covered by *Herschel*/SPIRE 350 and 500 μm, (OT2-sserje01-2, PI: S. Serjeant), and this work. Overlaid areas are: violet circle is the *GALEX* (GI4-057001-AKARI-NEP, PI: M. Malkan), cyan dashed and solid squares are the CFHT optical surveys from Oi et al. (2014), blue rectangle for CFHT NIR Y, J, and Ks, red solid and dashed circles are *AKARI* (NEP-Wide: Kim et al. 2012, and NEP-Deep: Takagi et al. 2012, respectively), black solid squares are the PACS (OT1-sserj01-1, PI: S. Serjeant), yellow solid circle is the Sub-mm of SCUBA-2 (Geach et al. 2017), green solid circle is WSRT radio 21 cm (White et al. 2010).

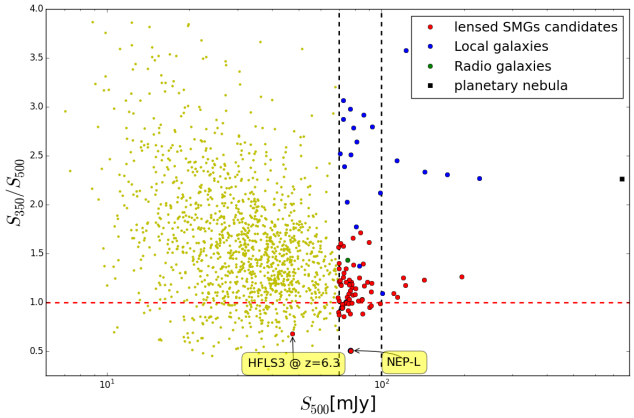

Figure 2. A color-flux diagram of *Herschel*/SPIRE photometry of all galaxies detected in the NEP-field with SNR > 3 at 500 μm. The vertical dashed lines are the selection limits at S_{500} > 100 mJy, and S_{500} > 70 mJy of our primary and supplementary lensed candidates respectively. The sources that satisfy the selection criteria are highlighted and classified as (red) gravitationally lensed source candidates at high-redshift, (blue) local galaxies, and (green) radio galaxies. The black square is the planetary nebula NGC 6543.

High-z sub-mm galaxies (SMGs) constitute an important population of massive systems in the early universe that have probably formed most of their stellar mass and heavy elements in intense, dust-enshrouded starbursts with high star formation rates, in the most massive dark matter halos. They are thought to be driven by major mergers of gas-rich galaxies at early epochs (e.g., Tacconi et al. 2008). But, it remains unknown how soon after the Big Bang such massive starburst progenitors appeared. So, by identifying these sources, we can learn more about the nature and properties of these populations in terms of their mass and redshift distributions; number densities; and environments that may present a challenge to current models of early cosmic structure formation (e.g., Negrello et al. 2010). According to the theoretical predictions of the evolutionary models such as those at 500 μm from, e.g., Negrello et al. (2007), the main populations of sources observed with flux densities above 100 mJy, consists of three populations: late-type galaxies at z > 0.1; flat-spectrum radio AGNs; and a significant fraction of bright strongly lensed SMGs at high redshift. Also, about 50% of galaxies with flux densities above 80 mJy are expected to be lensed SMGs, and the rest can be easily identified as local galaxies or as radio-loud AGNs from shallow optical imaging and radio surveys respectively. This method has been shown to be efficient at making a robust list of gravitationally lensed candidates high redshift galaxies.

5. THE SELECTION WITH *HERSCHEL*-SPIRE

Taking advantage of this method, we used our *Herschel* SPIRE data to build a list of gravitationally lensed source candidates. The identification of gravitationally lensed galaxies is performed by searching for bright and red sources via a selection in the far-IR color-flux diagram. A similar procedure is used by, e.g., Wardlow et al. (2013). We start by using the SPIRE 500 μm to select the lensed SMG candidates with a cut $S_{500\mu m}$ > 100 mJy (Figure 2). For further studies, we make also a supplementary candidate with flux (70 ≥ $S_{500\mu m}$ [mJy] ≥ 100), where 50% of galaxies are expected to be lensed SMGs (Negrello et al. 2010). A relatively low contamination from unlensed galaxies can be present in the candidate list. The primary contamination are late-type galaxies at z > 0.1 (Serjeant et al. 2005), and flat-spectrum radio quasars (or blazars) at higher redshifts ($z \gtrsim 1.0$) (Gonzalez et al. 2010). Both types of galaxies can have similar color to the high-redshift galaxies, but they can easily be identified from shallow optical and radio surveys. Local galaxies are discarded from the initial list by searching the spatially resolved galaxies in the optical catalog from Oi et al. (2014), and

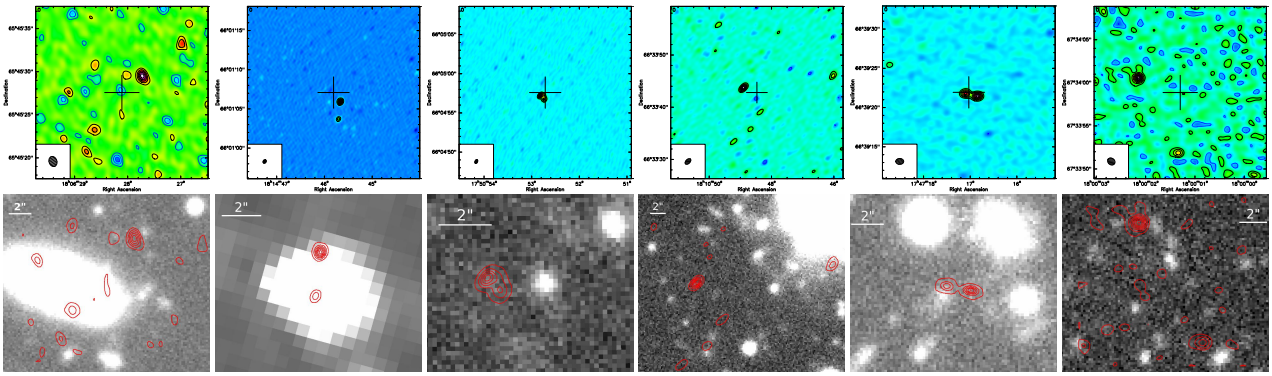

Figure 3. Upper panel: Images of the 1.3 mm continuum of our lensed candidates from NOEMA. The sources (from top left to bottom right) are NEP-05, NEP-09, NEP-12, NEP-23, NEP-25, and NEP-52. The images show evidence of multiple features in 3 sources (NEP-09, NEP-12, and NEP-25). Two others, (NEP-23, and NEP-52), are extended and display distinct lensed morphologies. Lower panel: The best available optical or near-IR images at the position of the candidate lensed SMGs. The overlaid red contours are from NOEMA 1.3 mm images. The sources (from top left to bottom right) are NEP-05, NEP-09, NEP-12, NEP-23, NEP-25, and NEP-52.

NASA/IPAC Extragalactic Database[1] at the position of the selected candidates. We found in total 18 bright low-redshift galaxies ($z < 0.1$), with various populations from spiral to starburst galaxies. Radio sources are discarded by searching for radio emission in the radio catalogs from VLA-NEP (Kollgaard et al. 1994) and WSRT (White et al. 2010).

The main list contains 6 sources with ($S_{500\mu m} > 100$ mJy), and 55 sources in the supplementary list with ($70 \geq S_{500\mu m}$ [mJy] ≥ 100). Assuming all of them are trustworthy high-redshift lensed galaxies would result in a surface density on the sky of ~ 0.44 deg^{-2}, and ~ 6.1 deg^{-2}, for the main and the supplementary candidate lists respectively. The number density of the main list is the highest among the values of previous studies (e.g., ~ 0.23 deg^{-2}, ~ 0.14 deg^{-2}, and ~ 0.26 deg^{-2} from Negrello et al. 2010, Wardlow et al. 2013 and Bussmann et al. 2013), respectively. The difference in the surface densities is not very significant from the statistical point of view, and it could be caused by cosmic variance.

6. IRAM-NOEMA INTERFEROMETRY

NOEMA (previously PdBI) is the most powerful millimeter radio telescope in the Northerm hemisphere that included eight 15-m diameter antennas, (at the time of the observing in 2016). The NOEMA configurations provide high angular resolutions up to 1.″6, 1.″1, 0.″4 at 230 GHz with point source sensitivities of 0.08–0.14 mJy. We obtained NOEMA continuum observations at 1.3 mm band, for 6 sources in our list of candidates. The observations were executed, (proposal W16DD, P.I.: F. Mazyed), during the Winter cycle 2016–2017, in conditions of good to excellent atmospheric phase stability (seeing $\sim 0.''1$ to $\sim 0.''3$). Band 3 (201–267 GHz) has been used with the WideX correlator, allowing to detect the continuum as well as any other emission lines, if present (but we had no line detections).

A first interesting result is that the *Herschel* sources can be divided into several components. This result is similar to what Karim et al. (2013) found using the Atacama Large Millimeter Array (ALMA). Faint SMGs in the 870-μm band derived from arcsecond-resolution observations with ALMA, like our NOEMA observations, allowed to get rid from the effects of confusion that we undergo with *Herschel*. However, their and our observations show that most of the brightest sources in our NEP sample are formed from the emission of multiple sources. Karim et al. (2013) suggested that the bright SMGs can be composed of multiple fainter SMGS. In all cases, NOEMA images have clearly identified the background lensed sources, but there is no indication for continuum emission from the foreground lenses. The identification of the lenses requires high spatial resolution (probably adaptive optics) observations at optical or NIR wavelengths. We used the most recent optical imaging of the SUBARU Hyper Suprime-Camera (HSC, Miyazaki et al. 2012; Goto et al. 2015). All the sources have optical imaging with HSC, except NEP9 which is out of HSC field-of-views (we used Spitzer IRAC 4.5 μm image). Figure 3 shows the best available optical or near-IR images at the position of the candidate lensed SMGs. The overlaid red contours from NOEMA 1.3 mm images are also shown. For all candidates, the background lensed source appears to be undetected in the optical images. Also for NEP9, it is hard to find any morphological structure that could be associated with the background source since the source is likely to be hidden behind the foreground source. This result confirms the high dust obscuration of these kind of galaxies, and that they would have been totally missed by standard optical/NIR imaging. On the other hand, the optical/NIR images support the idea of a gravitational lensing hypothesis. According to Figure 3, the image separations suggest the presence of a gravitational potential wells, for the lenses, typical of isolated galaxies (for NEP5 and NEP9), or small numbers of galaxies (for the other sources).

The final interpretation of the results is still uncertain. Given that we do not have enough information, yet, it is still impossible to apply a simple lensing model to estimate the basic parameters (e.g., deflection, distortion, amplification and time delay). Indeed, we would at least the ratio of the distances of the lens and lensed galaxies.

[1] https://ned.ipac.caltech.edu/

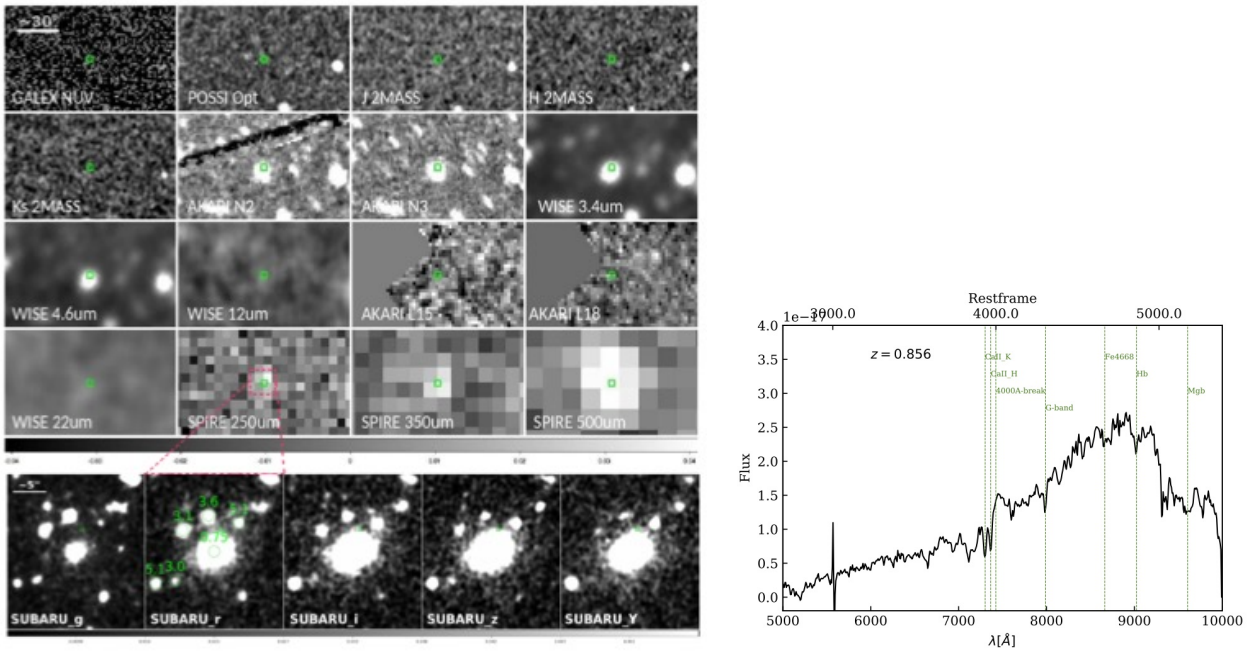

Figure 4. Left: Mosaic from the far-UV to the far-IR showing NEP-L. The upper panel shows detections of an object in the near-IR from 2 to 12 μm that is now confirmed to be a massive galaxy at $z_{\rm spec} = 0.856$ (right panel). And in the Far-IR from 250 to 500 μm that can be a high-redshift lensed galaxy. Lower panel : The deep HSC/SUBARU observations for this object (Goto et al. 2015), confirm that the central bright source is the lens, a massive (maybe) elliptical galaxy. In the r-band image are superimposed the photometric redshifts with the two possible optical counterparts at $z \sim 5.1$. Right: Gemini GMOS spectrum of the lens.

7. NEP-LEFT

NEP-Left (NEP-L) is our best candidate gravitational lensed galaxy at high redshift. Figure 4 shows the SED over different bands for NEP-L region. At the location of NEP-L, we have detections in the optical, NIR and MIR. However, no strong emission is detected, in the other band in X-rays, ultraviolet (UV) and radio. This source is not compatible with a local galaxy, or with a blazar that could produce such a rising far-infrared SED. Therefore, the best alternate explanation is that NEP-L is a high-redshift gravitationally-lensed galaxy. The lensing nature is supported by the fact that the MIR SED is not compatible with the FIR SED. We have not been able to find a satisfactory complete SED fitting using CIGALE. We definitely need to have two different objects at different redshifts. This anomalous is in agreement with the hypothesis mentioned in Rowan-robinson et al. (2014): 11 per cent of 500 μm selected sources are good lensing candidates.

Finally, from additional data, we can safely conclude that, it is very likely that we have a galaxy-galaxy gravitational lensing, and that the very bright source detected at the optical to mid-IR emission is the lens at $z_{\rm phot} \simeq 0.856$ (Figure 4) and that the source producing the FIR emission is the lensed one at $z_{\rm phot} \simeq 5.1$. But still more information are needed to understand NEP-L. Some very recent SMA observations of NEP-L have been secured and are now under processing. NOEMA observations will also be carried out by May 2018.

ACKNOWLEDGMENTS

We thank Johan Richard for his help in the interpretation of the Gemini GMOS spectra.

REFERENCES

Bouwens, R. et al. 2016, ApJ 830, 67
Burgarella, D. et al. 2005, MNRAS 360, 1413
Burgarella, D. et al. 2007, MNRAS 380, 986
Burgarella, D. et al. 2013, A& A 554, A70
Bussmann et al. 2013, ApJ 779, 1
Geach et al. 2017, MNRAS 465, 1789
Gonzalez et al. 2010, A& A 518, L38
Goto, T. et al. 2015, arXiv:1505.00012
Gruppioni, C. et al. 2013, MNRAS 432, 23
Karim et al. 2013, MNRAS 432, 2
Kollgaard et al. 1994, APJS 93, 145
Kim et al. 2012, A& A 548, 29
Miyazaki et al. 2012, SPIE 8446, 0
Negrello et al. 2010, Science 330, 800
Negrello et al. 2007, MNRAS 377, 1557
Noll, S. et al. 2009, A& A 507, 1793
Oi, N. et al. 2014 A& A 566, 60
Rowan-Robinson, M. et al. 2014, MNRAS 445, 3848
Serjeant, S. et al. 2005, MNRAS 356, 192
Tacconi et al. 2008, ApJ 680, 1
Takagi et al. 2012, A& A 537, A24,
Wardlow, J. et al. 2013, ApJ 762, 59
White et al. 2010 A& A 517, A54